Physics and Imaging in Radiation Oncology 12 (2019) 56–62

Contents lists available at ScienceDirect

Physics and Imaging in Radiation Oncology

journal homepage: www.elsevier.com/locate/phro

Original Research Article

Robust maximization of tumor control probability for radicality constrained radiotherapy dose painting by numbers of head and neck cancer

Eric Grönlund[a,b,*], Erik Almhagen[a,c], Silvia Johansson[d,e], Erik Traneus[f], Anders Ahnesjö[a,e]

[a] Medical Radiation Sciences, Department of Immunology, Genetics and Pathology, Uppsala University, Uppsala, Sweden
[b] Section of Medical Physics, Mälar Hospital, Eskilstuna, Sweden
[c] The Skandion Clinic, Uppsala, Sweden
[d] Experimental and Clinical Oncology, Department of Immunology, Genetics and Pathology, Uppsala University, Uppsala, Sweden
[e] Uppsala University Hospital, Uppsala, Sweden
[f] RaySearch Laboratories AB, Stockholm, Sweden

ARTICLE INFO

Keywords:
Dose painting
Dose painting by numbers
Head and neck cancer
^{18}FDG-PET/CT

ABSTRACT

Background and purpose: Radiotherapy with dose painting by numbers (DPBN) needs another approach than conventional margins to ensure a geometrically robust dose coverage for the tumor. This study presents a method to optimize DPBN plans that as opposed to achieve a robust dose distribution instead robustly maximize the tumor control probability (TCP) for patients diagnosed with head and neck cancer.

Material and methods: Volumetric-modulated arc therapy (VMAT) plans were optimized with a robust TCP maximizing objective for different dose constraints to the primary clinical target volume (CTVT) for a set of 20 patients. These plans were optimized with minimax optimization together with dose-responses driven by standardized uptake values (SUV) from ^{18}F-fluorodeoxyglucose positron emission tomography (^{18}FDG-PET). The robustness in TCP was evaluated through sampling treatment scenarios with isocenter displacements.

Results: The average increase in TCP with DPBN compared to a homogeneous dose treatment ranged between 3 and 20 percentage points (p.p.) which depended on the different dose constraints for the CTVT. The median deviation in TCP increase was below 1p.p. for all sampled treatment scenarios versus the nominal plans. The standard deviation of SUV multiplied by the CTVT volume were found to correlate with the TCP gain with $R^2 \geq 0.9$.

Conclusions: Minimax optimization of DPBN plans yield, based on the presented TCP modelling, a robust increase of the TCP compared to homogeneous dose treatments for head and neck cancers. The greatest TCP gains were found for patients with large and SUV heterogeneous tumors, which may give guidance for patient selection in prospective trials.

1. Introduction

The concept “dose painting” [1] in radiotherapy (RT) embed the hypothesis that it is beneficial to prescribe a spatially varying dose distribution based on predicted dose response variations acquired from functional imaging. For head and neck cancer it has in several studies been shown that increasing standardized uptake values (SUV) from ^{18}F-fluorodeoxyglucose positron emission tomography (^{18}FDG-PET) correlate with an increased recurrence risk after RT [2–7]. As noted in a review by Bentzen and Grégoire [8], the simplest image based dose prescription is an ad hoc linear mapping of image data into doses within suitable dose ranges, as used in several planning studies [9–19]. However, the same reviewers stated that the dose prescription ideally should be based upon empirical observations of pre-RT functional image data with post-RT dose-responses. One example of such an empirical approach have been presented by Vogelius et al. [5]. In their study they analyzed post-RT recurrence frequencies for different tumor regions defined by pre-RT ^{18}FDG-PET image data, and derived dose-response functions for use in a planning study of dose painting by contours for head and neck cancer. Followed by the approach from Vogelius et al. [5], we performed a retrospective analysis of the spatial relation between pre-RT SUV and post-RT recurrences and derived voxel specific SUV driven “dose painting by numbers (DPBN [20])” prescriptions for head and neck cancer [4]. These dose prescriptions were derived with the objective to maximize the tumor control probability (TCP) with the target volumes average dose constrained to that

* Corresponding author at: Medicinsk fysik och teknik, Mälarsjukhuset, SE – 631 88, Eskilstuna, Sweden.
E-mail address: eric.gronlund@regionsormland.se (E. Grönlund).

https://doi.org/10.1016/j.phro.2019.11.004
Received 3 September 2019; Received in revised form 10 November 2019; Accepted 20 November 2019

for conventional homogeneous treatments. However, we did not extensively analyze the deliverability of the resulting "ideal" dose prescriptions (i.e. the dose values were locally assigned by neglecting radiation transport, beam shaping, patient setup limitations, and TCP function uncertainties).

To investigate the feasibility of DPBN to increase the TCP in a clinical scenario, the resulting dose prescriptions must be expressed as clinically deliverable dose plans. Robust procedures are hence needed to consider the effect of geometrical uncertainties on the prescribed heterogeneous dose distributions. Sterpin et al. [21] have proposed a method to construct geometrically robust DPBN plans from a given ideal dose prescription. In their approach they firstly dilate an ideal dose prescription, followed by a deconvolution to mitigate effects of systematic and random geometrical uncertainties, respectively. These steps yield a dose distribution from which the final dose plan could be optimized towards. However, the method from Sterpin et al. [21] relies on the "static dose cloud approximation", i.e. that temporal changes of the anatomy has no impact on the spatial distribution of dose in the machine frame of reference [22,23]. A more general method to ensure geometrical robustness for treatment planning is minimax optimization. The minimax concept dates back to the first half of the 20th century [24] and is commonly used for decision making in e.g. game theory. For RT, minimax optimization is based upon a set of simulated scenarios of e.g. geometrical displacements of the isocenter and minimizes the objective value (that aims to be minimized) for the worst-case scenario [23,25]. The method is a general approach to achieve robust results for any reasonable treatment modality and objective function and should hence also apply for the optimization of dose painting plans.

In this study we have combined minimax optimization with the dose-response driven dose painting formalism given by Grönlund et al. [4,26]. We have also taken measures to investigate the influence of uncertainties for the dose-response functions used for robust DPBN optimization. The aim was to evaluate the potential and robustness to increase the TCP with clinically deliverable robustly optimized DPBN plans as compared to conventional homogeneous dose plans for patients diagnosed with head and neck squamous cell carcinoma.

2. Materials and methods

A set of DPBN plans was optimized with a planning objective that maximized the TCP under different mean target dose constraints for patients with head and neck squamous cell carcinoma. The TCP maximizing objective was implemented in a treatment planning system (TPS) and was based upon the method formulated by Grönlund et al. [4], where SUV from ^{18}FDG-PET are mapped to voxel specific dose-response functions. To ensure robustness with respect to isocenter positioning uncertainties, we utilized robust minimax optimization [23,25]. To test the robustness of both the dose distributions and the predicted TCP increases, we simulated a multitude of treatment scenarios by computing perturbed dose distributions resulting from random displacements of the planning isocenter. For a representative subset of the patients the additional impact of potential uncertainties of the SUV driven dose-response functions was also investigated.

2.1. Patient data for dose planning

A total of 20 patients treated with RT for head and neck squamous cell carcinoma were included. All of these had undergone ^{18}FDG-PET/CT imaging before RT and had target volumes and risk organs segmented according to clinical protocols. The included patients constituted a subset of the 59 patients used as a learning set to derive ideal dose painting prescriptions in our previous study [4,26] (Uppsala board ethical approval reference number 2014/287). These ideal dose painting prescriptions were optimized to maximize the TCP for the CTVT under the requirement of equal average dose to the CTVT as for the conventional homogeneous dose treatment of 70.1 Gy given to the learning set patients [4]. The ideal dose painting prescriptions did not consider radiation transport phenomena, dose delivery uncertainties, or uncertainties of the dose-response functions. The 20 patients were selected out of the 59 learning set patients on the basis to evenly represent the range of TCP increases compared to a homogeneous dose resulting from the ideal dose painting prescriptions of the learning set.

2.2. Integration of robust TCP maximization into a TPS

We implemented the SUV based dose-response functions from our previous work [4,26] into a research version of a TPS (RayStation v. 5.99.50.54, RaySearch Laboratories AB, Stockholm) for use as a dose painting objective to maximize the TCP for the primary tumor target volume (CTVT). Under the assumption of voxel independency, the TCP was calculated as the product of voxel specific TCP values $\mathrm{TCP}_{\mathrm{vox}}$ for the voxels belonging to the target volume (i.e. the CTVT). Since RayStation optimizes the dose by minimizing planning objective scalars, we formulated the SUV based TCP maximizing objective as

$$\underset{d}{\text{minimize}} \quad 1 - \prod_{\mathrm{vox}\in\mathrm{CTVT}} \left(\mathrm{TCP}_{\mathrm{vox}}\left(D_{\mathrm{EQD_{2Gy}}}(d),\mathrm{SUV}\right)\right)^{f_{\mathrm{vox}}} \tag{1}$$

where $\mathrm{TCP}_{\mathrm{vox}}$ is the voxel specific dose-response function which is a function of the voxel's dose in EQD_2 (equivalent dose in 2 Gy fractions) and SUV. The dose in EQD_2 was determined from the physical dose d with $\alpha/\beta = 10$ Gy. Moreover, f_{vox} is the fraction of a voxel that is within the CTVT. The $\mathrm{TCP}_{\mathrm{vox}}$ functions had been derived in our earlier study [4], given as

$$\mathrm{TCP}_{\mathrm{vox}}(d,\mathrm{SUV}) = \left(1 + \left[\frac{D_{50}(\mathrm{SUV})}{D_{\mathrm{EQD_{2Gy}}}(d)}\right]^{4\gamma_{50}}\right)^{-1} \tag{2}$$

where

$$D_{50}(\mathrm{SUV}) = D_{\mathrm{h}}\cdot\left((1 - a\cdot\mathrm{SUV})^{-b} - 1\right)^{1/4\gamma_{50}} \tag{3}$$

with $D_{\mathrm{h}} = 70.1$ Gy EQD_2 (representing the mean dose given to the patients of the learning set [4]), $a = 1.083\cdot10^{-2}$ (the slope of the local control ratio [4,26]), $b = 2.900\cdot10^{-3}$ (the normalizing exponent denoted as 'k' in [4,26]), and finally $\gamma_{50} = 1.659$. The values of a, b and γ_{50} include corrections for a normalization error of the SUV data in [4] as described in [26]. Furthermore, for robust minimax optimization we included the planning objective given in Eq. (1) into the optimization problem that the TPS strives to fulfill

$$\begin{aligned} \underset{d}{\text{minimize}} \quad & \left(\max_{k}\left[\sum_{i=1}^{n} w_i f_i(d_k)\right] + \sum_{i=n+1}^{n+m} w_i f_i(d)\right) \\ \text{subject to} \quad & \begin{cases} c_q(d_k) \leqslant 0, & \begin{cases} q = 1,\ldots,Q \\ k = 1,\ldots,K \end{cases} \\ c_j(d) \leqslant 0, & j = 1,\ldots,J \end{cases} \end{aligned} \tag{4}$$

where w_i is the importance weight for the planning objective f_i, n is the number of objectives used with minimax optimization, m is the number of objectives used without minimax optimization, Q is the number of constraints c_q used with minimax optimization, and J is the number of constraints c_j used without minimax optimization. The minimax part of the optimization selects, for each iteration, the maximum value out of K dose error scenarios d_k, i.e. the worst-case scenario is the one minimized. See Table 1 for specification of the used objectives and constraints.

2.3. Set up of treatment plans

For each patient we optimized four volumetric-modulated arc therapy (VMAT) plans with: the intention of delivery for 35 fractions without any adaptive modifications between the fractions; 2 arcs completing a full rotation; 6 MV photons from a Versa HD™ linear accelerator; and the dose calculated on a grid with 3.0 × 3.0 × 2.5 mm^3

Table 1
The objectives and constraints used for optimizing the three sets of DPBN plans with a mean dose constraint to the CTVT of either 70 Gy, 75 Gy or not applied (N/A). The weighting factor for the dose painting objective "maximize TCP" is set to unity, the other weighting factors are given relative to this objective.

Optimization objectives and constraints			
Structures	Objective	Weighting factor	Robustness distance
CTVT	maximize TCP	1	0.5 cm
	$D_{98\%} \geq 60$ Gy	Constraint	0.5 cm
	$D_{1cc} \leq 84$ Gy	Constraint	0.5 cm
	$D_{mean} = 70$ Gy or 75 Gy or N/A	Constraint	0.5 cm
Therapeutic nodes; PTVN-T	$D_{98\%} \geq 66.5$ Gy	350	N/A
	$D_{2\%} \leq 73.5$ Gy	150	N/A
Prophylactic nodes; PTVN-P	$D_{98\%} \geq 47.5$ Gy	350	N/A
	$D_{2\%} \leq 52.5$ Gy	150	N/A
Spinal cord	$D_{2\%} \leq 46$ Gy	Constraint	0.5 cm
Mandible	$D_{2\%} \leq 72$ Gy	5	N/A
	$D_{mean} \leq 65$ Gy	5	N/A
Parotid	$D_{mean} \leq 26$ Gy	5	N/A
Esophagus	$D_{mean} \leq 34$ Gy	5	N/A
Larynx	$D_{mean} \leq 44$ Gy	5	N/A
External	Dose falloff: 70–14 Gy for 1.5 cm	20	N/A

voxels. Of these four plans, one reference plan was optimized with a homogeneous dose of 70 Gy to the PTVT (i.e. the CTVT expanded with the clinically used PTV margin of 0.5 cm), while the other three plans were optimized as TCP maximized DPBN plans under various constraint settings. Two constraints were used for all three DPBN plans: a hot spot limitation constraint of $D_{1\,cm^3} \leqslant 84$ Gy physical dose for the CTVT (based on the study from Olteanu et al. [27]); and a minimum allowed dose to the CTVT of $D_{98\%} \geqslant 60$ Gy to allow for a dose reduction to regions with low SUV. Furthermore, for two DPBN plans we constrained the mean dose for the CTVT to either 70 Gy (based on the conventional homogeneous treatment dose for these patients), or 75 Gy as a dose escalation test. For the third DPBN plan we used the maximum dose constraint of $D_{1\,cm^3} \leqslant 84$ Gy only. The minimax optimization was used with an isocenter position uncertainty of 0.5 cm (denoted as robustness distance in Table 1) and was based on the clinically used CTVT-to-PTVT margin of 0.5 cm. For this robustness distance, the minimax optimization utilized 7 error scenarios of the isocenter positioning in the cardinal directions (i.e. 7 error positions by including the nominal isocenter position). Furthermore, the intended dose to the lymph node target volumes were not optimized with DPBN but set to 70 Gy for the therapeutic lymph nodes (PTVN-T) and 50 Gy for the prophylactic lymph nodes (PTVN-P). To avoid conflicting objectives, all overlap between the lymph node volumes and the CTVTs was removed with a margin of 0.5 cm (i.e. the lymph node volumes were reduced but the CTVTs were preserved in their original state). See Table 1 for further details of the used objectives for dose optimization.

2.4. Evaluation of robustness of TCP and dose criteria

We evaluated the robustness in TCP predictions and fulfilled dose criteria for all DPBN plans and for all 20 patients through simulating treatment scenarios with displacements of the isocenter. For this process we sampled a systematic displacement $\mathbf{x}_\Sigma$ for all 35 fractions, and for each fraction a random additional displacement $\mathbf{x}_\sigma$ that yielded the total displacement per fraction of $\mathbf{x}_{frac} = \mathbf{x}_\Sigma + \mathbf{x}_\sigma$. The total treatment dose (i.e. the dose for a treatment scenario) was hence calculated as the sum of the sampled fraction doses. The values of $\mathbf{x}_\Sigma$ and $\mathbf{x}_\sigma$ were sampled from isotropic 3D-Gaussian distributions with zero mean and standard deviations of 0.19 cm for $\mathbf{x}_\Sigma$ and 0.13 cm for $\mathbf{x}_\sigma$. These values were calculated (according to van Herk et al. [28]) by using data of the pre-CBCT setup positioning and the post-CBCT setup correction acquired for several fractions (in average for 10 fractions) for 58 head and neck cases treated at Uppsala University hospital. A total of 25 treatment scenarios were sampled, requiring in total $25 \times 35 = 875$ fraction specific dose calculations per plan.

2.5. Evaluation of the impact on the TCP by dose-response uncertainties

The impact on the potential to increase the TCP with DPBN due to inherent uncertainties in the voxel specific TCP_{vox} function given in Eqs. (2–3) was analyzed. For this analysis we derived a set of perturbed TCP_{vox} functions under the assumption that the recurrence frequency of the learning set data either was increased or decreased by one standard deviation from the observed recurrence frequency for the original learning set (given in [4]). We used these perturbed TCP_{vox} functions in Eq. (1) and optimized a new set of DPBN plans for a subset of the patients (6 patients).

3. Results

Based on the optimized DPBN plans we found that the TCP in comparison to the TCP for the homogeneous dose plans increased with the average of 3 percentage points (p.p.) (range 0–9p.p.), 12p.p. (range 2–27p.p.), and 20p.p. (range 4–45p.p.), for the optimizations with the mean dose constrained to 70 Gy, 75 Gy and not constrained, respectively (see Fig. 1). The TCP increases were found to correlate with the standard deviation of SUV multiplied by the volume of the CTVT, i.e. larger and more heterogeneous tumors had a greater potential for TCP increases (linear fits with the corresponding R^2 values are included in Fig. 1). It was also clear that the patients with the poorest prognosis for a homogeneous dose received the greatest TCP increases (see Fig. 1). Furthermore, regarding the impact of utilizing perturbed dose-response functions during the TCP maximization, it was found that it affected the TCP predictions (see Fig. 1) but had a very low impact on the resulting optimized dose distributions.

The robustly optimized DPBN plans were found to have consistently robust TCP values with a median deviation below 1p.p. for all 25 sampled treatment scenarios per plan and patient. The maximum observed deviation in TCP increase for a single scenario was 3.5p.p., found for a patient's plan optimized without a mean dose constraint where the nominal plan had a TCP increase of 18.6p.p. Moreover, Fig. 2 show dose-volume coverage maps (DVCM) for the spinal cord and the parotid belonging to all 20 patients, where the constraint of $D_{2\%} \leq 46$ Gy was consistently fulfilled for the spinal cord of each patient. However, the objective for the parotid of $D_{mean} \leq 26$ Gy was not always fulfilled.

For one of the included patients are the resulting VMAT planned voxel doses versus SUV shown (Fig. 3). For comparison are also the ideal voxel doses shown (i.e. voxel doses optimized to maximize the TCP for the CTVT for the same planning constraints but without considering radiation transport phenomena or geometric uncertainties). As expected, the TCP for the ideal voxel doses was slightly larger than for the robustly optimized DPBN plans.

4. Discussion

Several aspects of dose painting need profound consideration before clinical implementation. Besides evidence from clinical trials that demonstrate a favorable improvement of the TCP and the normal tissue complication probability (NTCP), the planning and delivery methods must ensure that the DPBN plans can be reliably delivered for clinical routine work. In this study we have focused on utilizing minimax optimization to achieve robustness for TCP and associated dose volume parameters for organs at risk. This approach is in contrast to other studies (such as Witte et al. [14] and Sterpin et al. [21]) that have

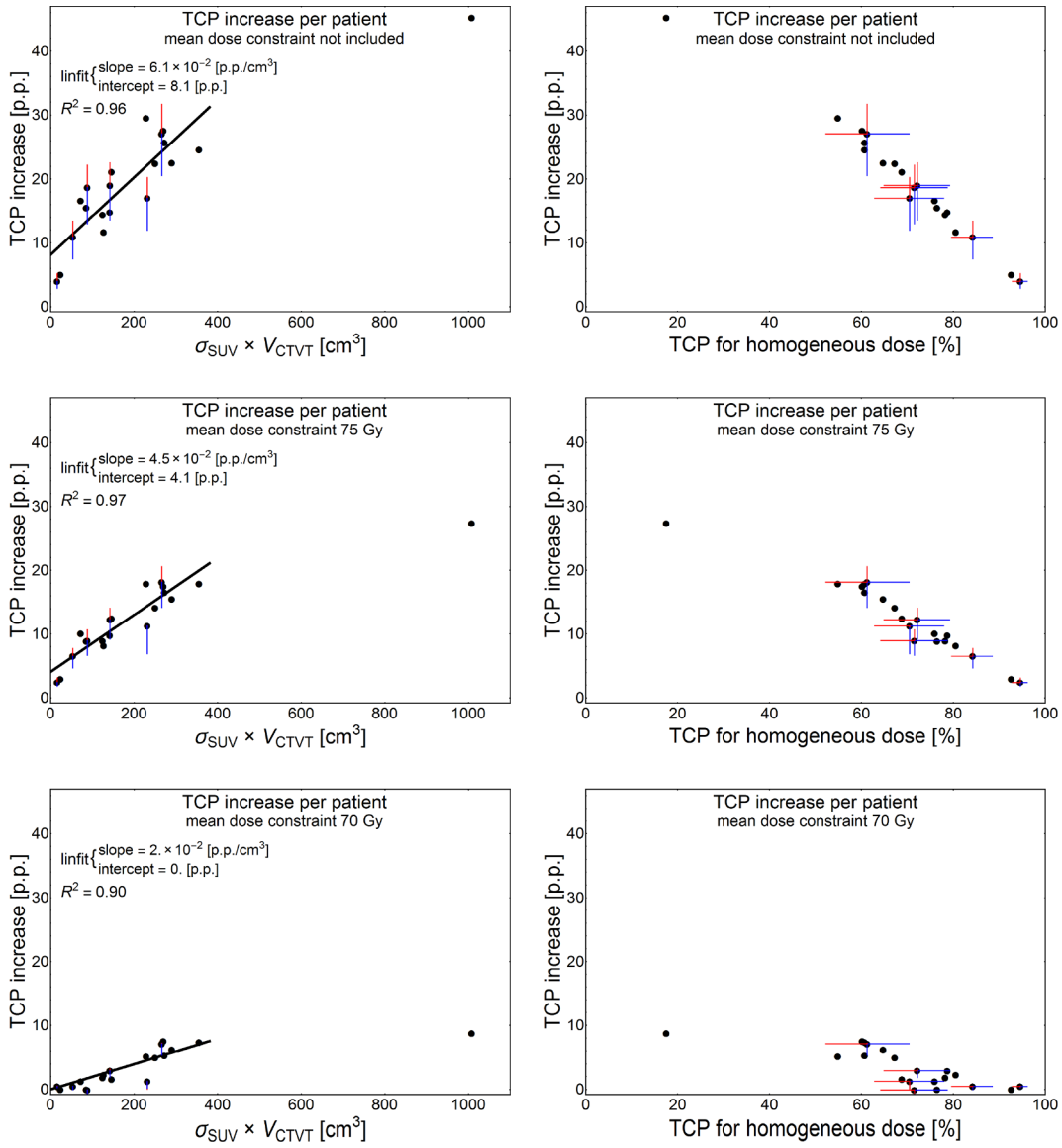

Fig. 1. The left column panels show TCP increases for the DPBN plans relative to the TCP for conventional plans with a homogeneous target dose of 70 Gy. These TCP increases are plotted versus the standard deviation of SUV multiplied by the CTVT volumes. Also shown are linear fits with the corresponding slope, intercept and R^2 values (the rightmost data point was excluded as an outlier for the fittings). The right column panels show the TCP increases for the DPBN plans in comparison to the TCP for the homogeneous dose plans with 70 Gy target dose. The panel rows differentiate the results for the DPBN plans without a mean dose constraint (uppermost), mean dose constraint 75 Gy (middle row), and 70 Gy (lowermost). Error bars are included in both columns (for a subset of six patients) where the red bars show results for a simulated decrease of the TCP for the learning set and vice versa for the blue bars (simulated with a decrease or increase of the learning set's TCP by one standard deviation for both cases). (For interpretation of the references to color in this figure legend, the reader is referred to the web version of this article.)

aimed to acquire robustness for a specific dose distribution. Our approach does however share some similarities with the study from Witte et al. [29] that implemented a planning objective that strived to optimize towards a high expectation value of the TCP by including both systematic and random uncertainties of the CTV positioning. Their approach did however utilize a Poisson dose-response modelling (based on Webb and Nahum [30]) and needed an accurate estimation of both the systematic and random uncertainties of the CTV positioning to ensure a robust TCP.

By sampling treatment scenarios with random displacements of the isocenter it was verified that the TCP increases for DPBN in comparison to the TCP for a homogeneous dose were robust. For the patient shown in Fig. 3, the predicted TCP decreased at worst by 4p.p. for the robustly optimized DPBN plans in comparison to the TCP for the ideal voxel dose prescriptions. Furthermore, it is likely that the intrinsic dose blurring caused by radiation transport processes is a larger cause for reducing the TCP gain with DPBN plan optimization as compared to the use of robust minimax optimization. We tested this for the patient presented in Fig. 3 by comparing the TCP for the ideal voxel doses versus the TCP for non-robustly optimized DPBN plans and found a decrease in TCP of 3p.p. as compared to at worst 4.p.p. for the robust DPBN plans. This observation may indicate that the minimax optimization does not cause a major decreasing effect on the achievable TCP gains.

The potential gains in TCP with robust DPBN, as illustrated in Fig. 1, indicate that larger and more heterogeneous tumors gain the highest TCP increases with dose painting, as predicted in our earlier article [4]. More speculative planning compromises could be investigated through explicit modelling and inclusion of normal tissue complication probabilities (NTCP), as suggested by e.g. Vogelius et al. [5]. We have not taken that step in our study, but instead used the maximum recommended target dose from Olteanu et al. [27] together with commonly used DVH limitation objectives (Table 1) to simplify

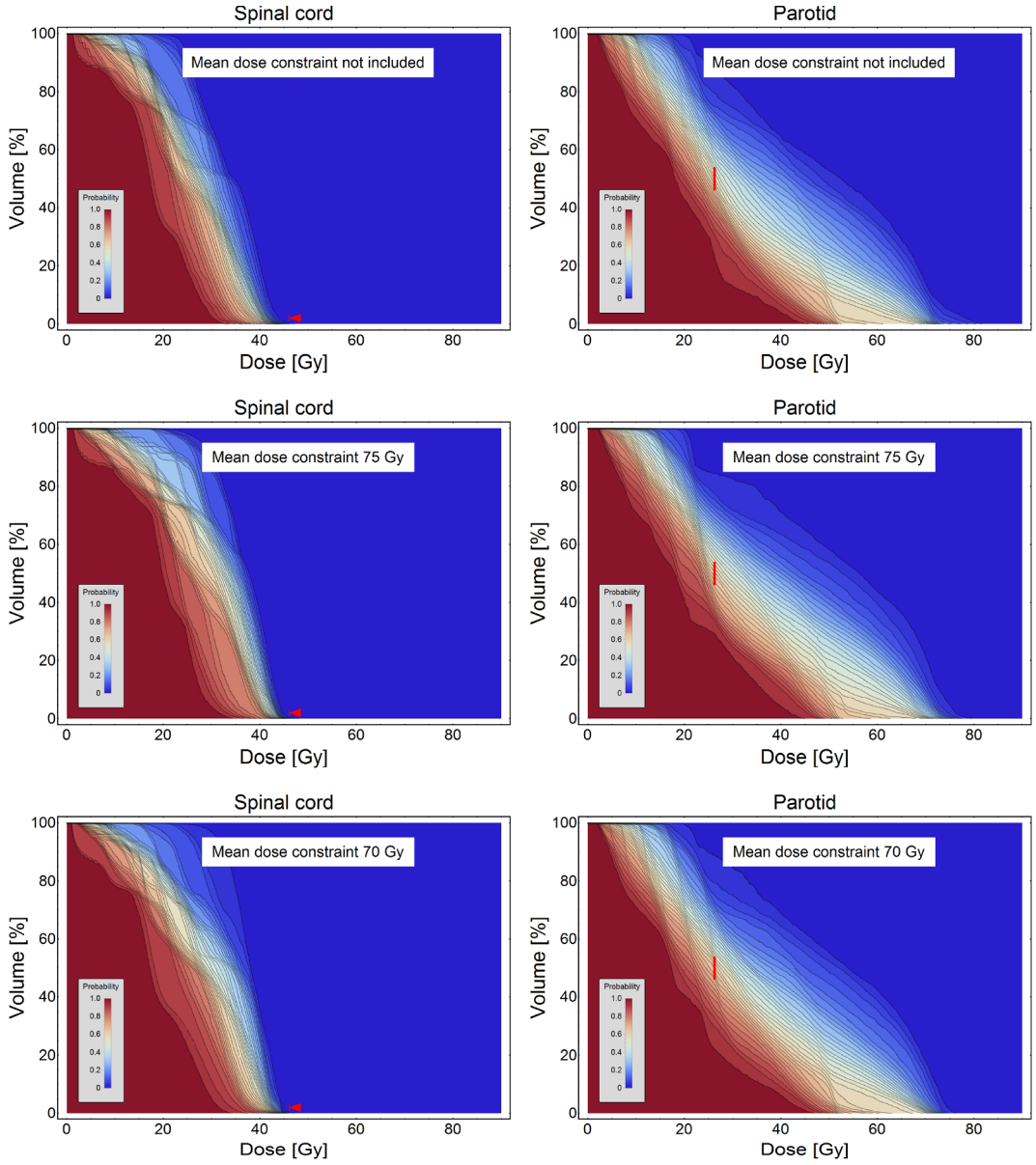

Fig. 2. The left column panels show dose volume coverage maps (DVCM) for the spinal cord of all 20 patients based on 25 treatment scenarios per plan, each including 35 fractions. The red arrows show the dose-volume constraint used for the spinal cord (i.e. $D_{2\%} \leq 46$ Gy). The right column panels show the corresponding DVCMs for the parotid volumes with the mean dose objective $D_{\text{mean}} < 26$ Gray marked as a red bar around 50% volume. The panel rows differentiate the results for the DPBN plans without a mean dose constraint (uppermost), 75 Gy mean dose constraint (middle row), and 70 Gy (lowermost). The unit probability area (reddish-brown color) marks the dose-volume region that were certain for all patients and all scenarios while zero probability (deep blue) show the dose-volume regions never actualized. (For interpretation of the references to color in this figure legend, the reader is referred to the web version of this article.)

comparisons with current clinical practice. As seen in Fig. 2, the spinal cord constraint $D_{2\%} \leq 46$ Gy was consistently fulfilled for all plans and treatment scenarios. However, for some patients the parotid volumes were overlapping with the CTVT or lymph nodes, which for these cases implied conflicting objectives where a dose coverage for the tumor target was prioritized.

Our study is based on a dose painting formalism where empirical correlations of pre-treatment image data with post-treatment recurrence locations is used for TCP modelling, as described in our earlier article [4] and corrected for a normalization error of the SUV data in [26]. One major assumption is that tumor control for a voxel is uncorrelated with all other voxels (as in Ebert and Hoban [31]). Another assumption is that the dose-response can be characterized with a logistic dose-response function driven by the parameters D_{50} and γ_{50} [3229], where D_{50} is assigned as a function of SUV from ^{18}FDG-PET (see Eqs. (2–3)), and γ_{50} is set constant as in Vogelius et al. [5]. An empirical SUV-dependent value of γ_{50}would have been more appealing but requires observed failure frequencies at different dose levels, which was not available from our learning set data. Large scale pooling of multi-institutional data could enable more elaborated dose-response modelling but was beyond the scope of this study. However, the impact on the TCP from potential recurrence uncertainties was evaluated by optimizing plans with a perturbed set of the voxel specific TCPvox functions. The results of optimizing with these perturbed functions are shown in Fig. 1, which demonstrate that if the TCP prediction for a homogeneous dose decrease the dose painting allows for almost all cases a larger TCP increase, and vice versa. These observations are more noticeable for the patients with a poorer prognosis and by escalating the allowed dose (see Fig. 1).

There may be uncertainties of using SUV from FDG-PET as a basis to

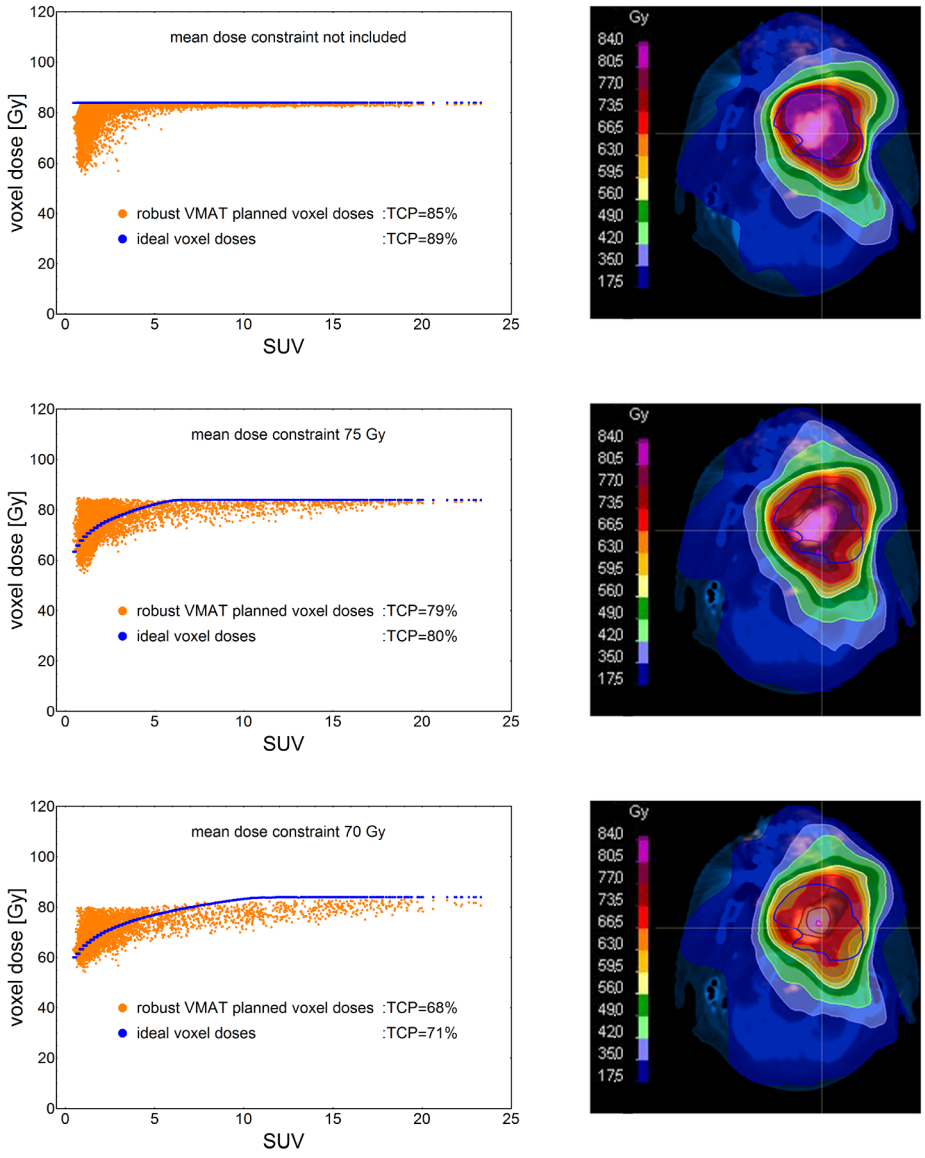

Fig. 3. The left column panels show the robustly planned VMAT voxel doses vs. SUV within the CTVT for one of the patients (the CTVT is marked by the blue contour in the right column). The corresponding ideal dose painting prescriptions are also shown (i.e. voxel doses vs. SUV optimized under the same constraints but without considering radiation transport phenomena or geometrical robustness). The right column shows the corresponding dose distribution overlaid on a fused PET/CT image slice for the same patient. The panel rows differentiate the results for the DPBN plans without a mean dose constraint (uppermost), 75 Gy mean dose constraint (middle row), and 70 Gy (lowermost). The TCP predictions for both the robust VMAT planned voxel doses and the ideal voxel doses are also shown. This patient had a TCP prediction of 61% for a homogeneous dose treatment with 70 Gy (not shown). (For interpretation of the references to color in this figure legend, the reader is referred to the web version of this article.)

optimize dose painting plans. However, in the review from Lodge et al. [33] they report that SUV is a highly replicable metric to quantify FDG-uptake. Moreover, Rasmussen et al. [34] analyzed the spatial and temporal impact on TCP predictions for a dose painting setting in comparison to the TCP for a conventional homogeneous dose. By using two different FDG-PET scans acquired with an interval of three days and using a logistic dose-response model, they found that the TCP prediction differed with less than 1% for 23 out of 24 patients. Furthermore, the TCP increases with dose painting versus a homogeneous dose from our earlier work [4] did not change much when the SUV was corrected for activity decay [26]. This indicates that the major driving force for TCP benefits with dose painting is the SUV heterogeneity, rather than the absolute values, also reported in [4] for a test with relative versus absolute SUV. All together, these findings suggest that, at least for the startup of a DPBN treatment, uncertainties of the ^{18}FDG-PET image data is not a major issue. However, we have not investigated whether adaptation of ^{18}FDG-PET driven dose painting optimization between treatment fractions is beneficial, although shown feasible by Duprez et al. [13].

Dose painting is still under development and has to our knowledge not yet been proved by clinical studies as an outcome-improving treatment technique. For example, Berwouts et al. [35] performed a long-term analysis of the outcomes for patients with head and neck cancer that either had been treated with dose painting or conventional IMRT. They found that dose painting increased the risks for toxicities but without significant improvement in outcomes as compared to the control group. However, their dose painting prescriptions was acquired from a linear mapping of SUV from ^{18}FDG-PET into voxel doses and did not explicitly involve optimization of the TCP or include considerations of the average dose to the target volumes.

Further studies are needed to test whether a direct application of an empirically driven dose painting formalism can improve the prospects for patients with head and cancer. It would indeed be compelling to test the presented dose-response functions on another independent set of patients with head and neck cancer and study whether the TCP prediction is in line with the observed TCP of such an independent patient cohort. If such a study would prove to be veracious, a next step would be to start a clinical trial. As an example, using the metric of $\sigma_{SUV} \times V_{CTVT} > 200$ cm^3 as inclusion criteria for a hypothetical trial, the estimated average TCP would, based on the presented data, increase from 63% (for a homogeneous treatment) to 76% (for the dose painting treatment with a mean dose constraint of 75 Gy). To detect this TCP difference, it would for 90% power and 5% level of significance require a study size of at least 215 patients in each arm. If such a trial would be successful, a final step would be to study whether DPBN is the true cause of the TCP increase.

In conclusion, robust minimax optimization of TCP with SUV driven dose-response functions can yield dose painting plans that demonstrate a robustly increased TCP versus homogeneous dose treatments for head and neck cancers. Potential inherent uncertainties of the SUV driven dose-response functions affect the TCP predictions but does still yield a TCP increasing potential. The TCP increases correlated with the volume and SUV heterogeneity of the tumors, which may give guidance for patient selection in prospective trials.

Conflict of interest statement

The authors declare the following financial interests/personal relationships which may be considered as potential competing interests: Erik Traneus is employed by RaySearch Laboratories AB.

The other authors declare no conflict of interest.

Acknowledgements

This research was supported by the Swedish Cancer Society, grant number 130632. We are grateful to Zahra Taheri Kadkhoda at Uppsala University Hospital for helpful discussions.

References

[1] Ling CC, Humm J, Larson S, Amols H, Fuks Z, Leibel S, et al. Towards multi-dimensional radiotherapy (MD-CRT): biological imaging and biological conformality. Int J Radiat Oncol 2000;47:551–60. https://doi.org/10.1016/S0360-3016(00)00467-3.

[2] Jeong J, Setton JS, Lee NY, Oh JH, Deasy JO. Estimate of the impact of FDG-avidity on the dose required for head and neck radiotherapy local control. Radiother Oncol 2014;111:340–7. https://doi.org/10.1016/j.radonc.2014.03.018.

[3] Due AK, Vogelius IR, Aznar MC, Bentzen SM, Berthelsen AK, Korreman SS, et al. Recurrences after intensity modulated radiotherapy for head and neck squamous cell carcinoma more likely to originate from regions with high baseline [18F]-FDG uptake. Radiother Oncol 2014;111:360–5. https://doi.org/10.1016/j.radonc.2014.06.001.

[4] Grönlund E, Johansson S, Montelius A, Ahnesjö A. Dose painting by numbers based on retrospectively determined recurrence probabilities. Radiother Oncol 2017;122:236–41. https://doi.org/10.1016/j.radonc.2016.09.007.

[5] Vogelius IR, Håkansson K, Due AK, Aznar MC, Berthelsen AK, Kristensen CA, et al. Failure-probability driven dose painting. Med Phys 2013;40:081717https://doi.org/10.1118/1.4816308.

[6] Kunkel M, Förster GJ, Reichert TE, Kutzner J, Benz P, Bartenstein P, et al. Radiation response non-invasively imaged by [18F]FDG-PET predicts local tumor control and survival in advanced oral squamous cell carcinoma. Oral Oncol 2003;39:170–7. https://doi.org/10.1016/S1368-8375(02)00087-8.

[7] Xie P, Yue JB, Fu Z, Feng R, Yu JM. Prognostic value of 18F-FDG PET/CT before and after radiotherapy for locally advanced nasopharyngeal carcinoma. Ann Oncol 2010;21:1078–82. https://doi.org/10.1093/annonc/mdp430.

[8] Bentzen SM, Gregoire V. Molecular imaging-based dose painting: a novel paradigm for radiation therapy prescription. Semin Radiat Oncol 2011;21:101–10. https://doi.org/10.1016/j.semradonc.2010.10.001.

[9] Alber M, Paulsen F, Eschmann SM, Machulla HJ. On biologically conformal boost dose optimization. Phys Med Biol 2003;48:N31.

[10] Das SK, Miften MM, Zhou S, Bell M, Munley MT, Whiddon CS, et al. Feasibility of optimizing the dose distribution in lung tumors using fluorine-18-fluorodeoxyglucose positron emission tomography and single photon emission computed tomography guided dose prescriptions. Med Phys 2004;31:1452–61. https://doi.org/10.1118/1.1750991.

[11] Vanderstraeten B, Duthoy W, Gersem WD, De Neve W, Thierens H. [18F]fluorodeoxy-glucose positron emission tomography ([18F]FDG-PET) voxel intensity-based intensity-modulated radiation therapy (IMRT) for head and neck cancer. Radiother Oncol 2006;79:249–58. https://doi.org/10.1016/j.radonc.2006.03.003.

[12] Rickhey M, Koelbl O, Eilles C, Bogner L. A biologically adapted dose-escalation approach, demonstrated for 18F-FET-PET in brain tumors. Strahlenther Onkol 2008;184:536–42. https://doi.org/10.1007/s00066-008-1883-6.

[13] Duprez F, De Neve W, De Gersem W, Coghe M, Madani I. Adaptive dose painting by numbers for head-and-neck cancer. Int J Radiat Oncol 2011;80:1045–55. https://doi.org/10.1016/j.ijrobp.2010.03.028.

[14] Witte M, Shakirin G, Houweling A, Peulen H, van Herk M. Dealing with geometric uncertainties in dose painting by numbers: Introducing the ΔVH1This work was supported by Dutch Cancer Society grant 2007–3895.1. Radiother Oncol 2011;100:402–6. https://doi.org/10.1016/j.radonc.2011.08.028.

[15] Berwouts D, Olteanu LAM, Duprez F, Vercauteren T, De Gersem W, De Neve W, et al. Three-phase adaptive dose-painting-by-numbers for head-and-neck cancer: initial results of the phase I clinical trial. Radiother Oncol 2013;107:310–6. https://doi.org/10.1016/j.radonc.2013.04.002.

[16] Differding S, Sterpin E, Janssens G, Hanin F-X, Lee JA, Grégoire V. Methodology for adaptive and robust FDG-PET escalated dose painting by numbers in head and neck tumors. Acta Oncol 2015:1–9. https://doi.org/10.3109/0284186X.2015.1046997.

[17] Arnesen MR, Knudtsen IS, Rekstad BL, Eilertsen K, Dale E, Bruheim K, et al. Dose painting by numbers in a standard treatment planning system using inverted dose prescription maps. Acta Oncol 2015;54:1607–13. https://doi.org/10.3109/0284186X.2015.1061690.

[18] Fontanarosa D, Witte M, Meijer G, Shakirin G, Steenhuijsen J, Schuring D, et al. Probabilistic evaluation of target dose deterioration in dose painting by numbers for stage II/III lung cancer. Pract Radiat Oncol 2015.

[19] Barragán AM, Differding S, Janssens G, Lee JA, Sterpin E. Feasibility and robustness of dose painting by numbers in proton therapy with contour-driven plan optimization. Med Phys 2015;42:2006–17. https://doi.org/10.1118/1.4915082.

[20] Bentzen SM. Theragnostic imaging for radiation oncology: dose-painting by numbers. Lancet Oncol 2005;6:112–7.

[21] Sterpin E, Differding S, Janssens G, Geets X, Grégoire V, Lee JA. Generation of prescriptions robust against geometric uncertainties in dose painting by numbers. Acta Oncol 2014:1–8. https://doi.org/10.3109/0284186X.2014.930171.

[22] Unkelbach J, Bortfeld T, Martin BC, Soukup M. Reducing the sensitivity of IMPT treatment plans to setup errors and range uncertainties via probabilistic treatment planning. Med Phys 2009;36:149–63. https://doi.org/10.1118/1.3021139.

[23] Unkelbach J, Alber M, Bangert M, Bokrantz R, Chan TCY, Deasy JO, et al. Robust radiotherapy planning. Phys Med Biol 2018;63:22TR02. https://doi.org/10.1088/1361-6560/aae659.

[24] von Neumann J, Morgenstern O, Rubinstein A. Theory of Games and Economic Behavior (60th Anniversary Commemorative Edition). Princeton University Press; 1944.

[25] Fredriksson A, Forsgren A, Hårdemark B. Minimax optimization for handling range and setup uncertainties in proton therapy: Minimax optimization for handling uncertainties in proton therapy. Med Phys 2011;38:1672–84. https://doi.org/10.1118/1.3556559.

[26] Grönlund E, Johansson S, Montelius A, Ahnesjö A. Corrigendum to “Dose painting by numbers based on retrospectively determined recurrence probabilities” [Radiother Oncol 122 (2017) 236–241]. Radiother Oncol 2018;2018. https://doi.org/10.1016/j.radonc.2018.11.004.

[27] Olteanu LAM, Duprez F, De Neve W, Berwouts D, Vercauteren T, Bauters W, et al. Late mucosal ulcers in dose-escalated adaptive dose-painting treatments for head-and-neck cancer. Acta Oncol 2018;57:262–8. https://doi.org/10.1080/0284186X.2017.1364867.

[28] van Herk M. Errors and margins in radiotherapy. Semin Radiat Oncol 2004;14:52–64. https://doi.org/10.1053/j.semradonc.2003.10.003.

[29] Witte MG, van der Geer J, Schneider C, Lebesque JV, Alber M, van Herk M. IMRT optimization including random and systematic geometric errors based on the expectation of TCP and NTCP. Med Phys 2007;34:3544–55. https://doi.org/10.1118/1.2760027.

[30] Webb S, Nahum AE. A model for calculating tumour control probability in radiotherapy including the effects of inhomogeneous distributions of dose and clonogenic cell density. Phys Med Biol 1993;38:653–66. https://doi.org/10.1088/0031-9155/38/6/001.

[31] Ebert MA, Hoban PW. Some characteristics of tumour control probability for heterogeneous tumours. Phys Med Biol 1996;41:2125. https://doi.org/10.1088/0031-9155/41/10/019.

[32] Bentzen SM, Tucker SL. Quantifying the position and steepness of radiation dose-response curves. Int J Radiat Biol 1997;71:531–42. https://doi.org/10.1080/09553097143860.

[33] Lodge MA. Repeatability of SUV in Oncologic 18F-FDG PET. J Nucl Med 2017;58:523–32. https://doi.org/10.2967/jnumed.116.186353.

[34] Rasmussen JH, Vogelius IR, Aznar MC, Fischer BM, Christensen CB, Friborg J, et al. Spatio-temporal stability of pre-treatment 18F-Fludeoxyglucose uptake in head and neck squamous cell carcinomas sufficient for dose painting. Acta Oncol 2015;54:1416–22. https://doi.org/10.3109/0284186X.2015.1061694.

[35] Berwouts D, Madani I, Duprez F, Olteanu LAM, Vercauteren T, Boterberg T, et al. Long-term outcome of ^{18} F-fluorodeoxyglucose-positron emission tomography-guided dose painting for head and neck cancer: Matched case-control study. Head Neck 2017;39:2264–75. https://doi.org/10.1002/hed.24892.